Journal of Low Temperature Physics manuscript No.
(will be inserted by the editor)

Quantifying the effect of cosmic ray showers on the X-IFU energy resolution

P. Peille[1] · **R. den Hartog**[2] · **A. Miniussi**[3] · **S. Stever**[4,5,6] · **S. Bandler**[3] · **C. Kirsch**[7] · **M. Lorenz**[7] · **T. Dauser**[7] · **J. Wilms**[7] · **S. Lotti**[8] · **F. Gatti**[9] · **C. Macculi**[8] · **B. Jackson**[2] · **F. Pajot**[10]

the date of receipt and acceptance should be inserted later

Abstract The X-ray Integral Field Unit (X-IFU) will operate an array of more than 3000 Transition-Edge Sensor pixels at 90 mK with an unprecedented energy resolution of 2.5 eV at 7 keV. In space, primary cosmic rays and secondary particles produced in the instrument structure will continuously deposit energy on the detector wafer and induce fluctuations on the pixels' thermal bath. We have investigated through simulations of the X-IFU readout chain how these fluctuations eventually influence the energy measurement of X-ray photons. Realistic timelines of thermal bath fluctuations at different positions in the array are generated as a function of a thermal model and the expected distribution of the deposited energy of the charged particles. These are then used to model the TES response to these thermal perturbations and their influence on the on-board energy reconstruction process. Overall, we show that with adequate heatsinking, the main energy resolution degradation effect remains minimal and within the associated resolution allocation of 0.2 eV. We further study how a dedicated triggering algorithm could be put in place to flag the rarer large thermal events.

Keywords X-IFU · X-ray microcalorimeters · TES · Cosmic rays · Energy resolution

1 Introduction

Planned for launch in the early 2030s onboard the *Athena* X-ray observatory [1], the X-ray Integral Field Unit [2] will operate an array of more than 3000 Transition Edge Sensor

Contact: Philippe Peille
E-mail: philippe.peille@cnes.fr

[1] CNES, 18 Avenue Édouard Belin, 31400 Toulouse, France
[2] SRON, Netherlands Institute for Space Research, Sorbonnelaan 2, 3584 CA Utrecht
[3] NASA/Goddard Space Flight Center, 8800 Greenbelt Rd, Greenbelt, MD 20771, United States
[4] Kavli IPMU (WPI), UTIAS, The University of Tokyo, Kashiwa, Chiba 277-8583, Japan
[5] IAS, INSU/CNRS, Bt. 121, Université Paris-Sud, Orsay, 91405, France
[6] LAL, IN2P3/CNRS, Bt. 200, Universiteé Paris-Sud, Orsay, 91405, France
[7] ECAP, University of Erlangen-Nuremberg Sternwartstr. 7 96049 Bamberg, Germany
[8] INAF/IAPS, Istituto di Astrofisica e Planetologia Spaziali at INAF, Via Fosso del Cavaliere 100, 00133, Roma, Italy
[9] Dept. of Physics, University of Genova, Genoa, Italy
[10] IRAP, Université de Toulouse, CNRS, UPS, CNES, Toulouse, France

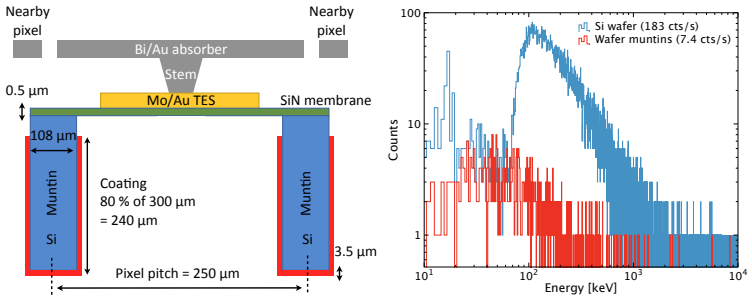

Fig. 1 *Left:* Schematic of the muntin structure suspending the TES array on a SiN membrane. A coating (typically gold) covers the bottom of each muntin as well as its side up to 80 % (limited by the deposition angle). Figure adapted with permission from [7]. *Right:* Spectrum of CR induced energy depositions in the Si frame and muntin structure. (Color figure online)

(TES) microcalorimeters providing an unprecedented energy resolution of 2.5 eV (FWHM at 7 keV) over a field of view of 5'. At its orbit around the L2 Lagrangian point, the X-IFU will be subject to a continuous flux of high energy Cosmic Rays (CR). The most energetic of these charged particles will go through the instrument structure, creating secondary particles in their passing. Primary and secondary particles will regularly deposit energy in the X-IFU pixels themselves and in the detector Si wafer frame. The former will create false events and generate the so-called instrument non X-ray background [3]. Most of it will be rejected by a cryogenic anticoincidence detector (cryoAC) located less than 1 mm away from the main detector [4]. Energy depositions in the wafer will induce heat waves across the wafer, which may perturb the pixels' signal and eventually the energy measurement of X-ray photons. This effect was critical for the *Planck/HFI* instrument [5] and this paper aims at estimating the impact of these CR induced thermal fluctuations on the X-IFU energy resolution.

2 Study inputs

2.1 Energy deposition in the X-IFU wafer

The X-IFU pixels are comprised of a Mo/Au TES and an overhanging Bi/Au absorber providing the required X-ray stopping power. The TESs themselves will be suspended on a Si wafer by a thin SiN membrane to create the appropriate weak thermal link to a ∼50 mK thermal bath. This suspension is created by a back-etch up to the SiN membrane, forming a muntin structure as shown in Fig. 1 (left). The expected energy deposition in both the Si wafer main frame and the muntin structure was characterized with an 83 s long Geant4 simulation performed under Solar minimum conditions (maximum GCR flux, [3]). Fig. 1 (right) shows the resulting spectra. With its surface of ∼63 cm^2, the Si frame sees a high count rate of 183 cts/s with an average deposited energy of ∼ 450 keV. In contrast, the smaller muntin structure (∼0.9 cm^2 top surface) receives only 7 cts/s with a mean impact energy of ∼ 250 keV. For simplicity, all individual energy depositions simulated by Geant4 from a single primary CR event, including that of the associated secondary particles, were summed together to create a single event. The impact of this hypothesis compared to resolving all depositions was studied in [6] and shown to moderately overestimate the final impact on the energy resolution.

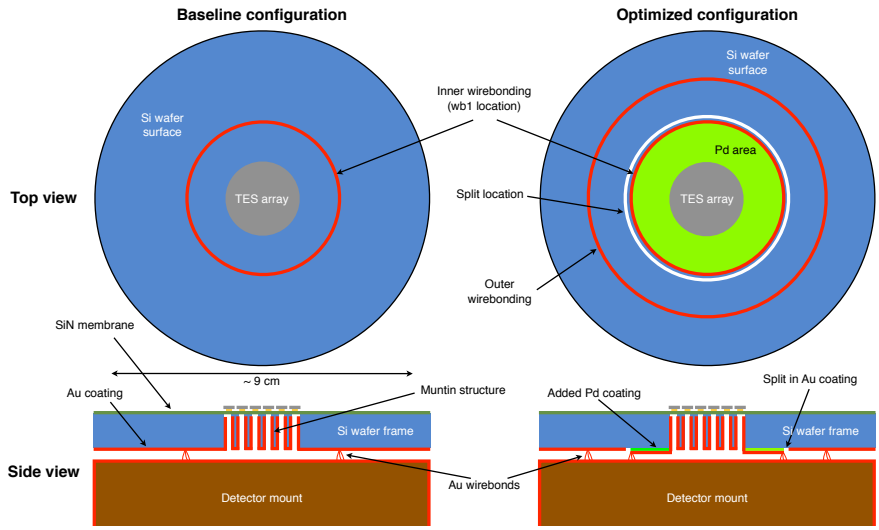

Fig. 2 The two studied heatsinkinking designs. For simplicity, the real geometries were approximated with centrally symmetric equivalents. *Left:* The baseline configuration with 1000 wirebonds around the perimeter of the cryoAC (*wb1* location) and a gold back coating of 3.5 μm thickness. *Right:* Optimized configuration with an additional Pd coating to dampen the thermal response near the TES array and a split in the Au coating on the frame to limit the conductivity towards the periphery. See more details in [7]. (Color figure online)

2.2 TES wafer thermal response

The X-IFU wafer thermal response was modeled and characterized in [7] (see also [6] for a similar simulation effort) for two heatsinking designs as a function of the CR impact position for a pixel at the center and at the edge of the TES array (see Fig. 2): the first configuration corresponds to the currently-baselined heatsinking approach with gold wirebonds connecting the wafer gold back coating (3.5 μm gold layer deposited on the back side of the wafer – see also Fig. 1) to the focal plane 50 mK structure around the perimeter of the cryoAC (*wb1* location). The second design has been optimized by adding on top of the gold coating a palladium layer close to the TES array to dampen the frame response. The wafer backside coating was also removed between the *wb1* location and an outer second wirebonding ring in order to cut the lateral thermal conductivity between the outer frame and the TES array.

Fig. 3 (left) shows a comparison of the simulated wafer thermal response in these two configurations. As expected from the high specific heat capacity of palladium, the optimized design shows smaller and slower temperature profiles for events close to the TES array, while the split in the backside coating efficiently cuts the events in the outer frame. Fig. 3 (right) in turn shows the response (simulated for the baseline design) to events in the muntin structure located directly below the TES detectors. In this case, we see very sharp temperature profiles, rising up to a significant fraction of a Kelvin, but decreasing below the μK level in ~ 1 ms.

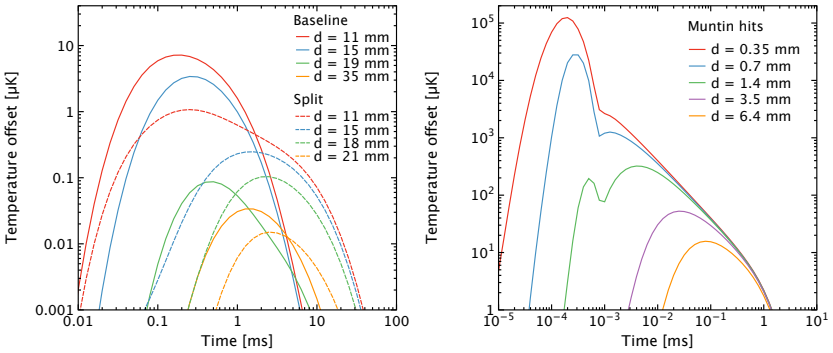

Fig. 3 Simulated temperature pulses measured at the center of the array for CR impacts at varying distances (500 keV). *Left:* Simulation of impacts in the Si frame for both studied heatsinking configurations. *Right:* Simulation of impacts in the muntin structure below the pixels. (Color figure online)

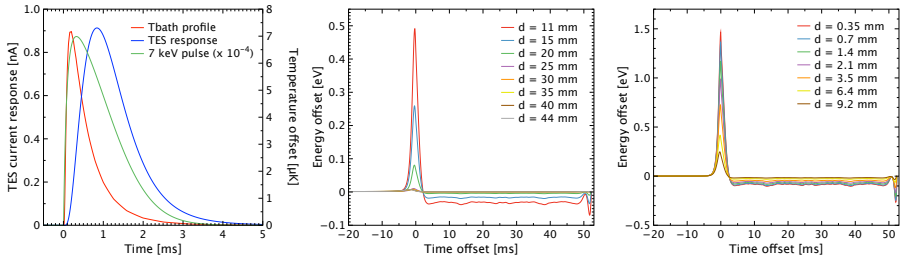

Fig. 4 *Left:* Response of a TES located at the center of the array to a frame CR impact at 11 mm distance (edge of the TES array) in the baseline heatsinking configuration (resulting temperature profile shown in red), compared to an X-ray pulse. *Middle and right:* Energy offset measured on a 7 keV X-ray event recorded in the central pixel from a CR event at varying time offset and distance for frame (middle) and muntin (right) hits. All profiles are shown for the baseline heatsinking design and for the average energy deposition (450 keV for the frame and 250 keV for the muntins). (Color figure online)

3 Effect on the X-IFU energy measurement

3.1 TES response to thermal fluctuations

The response of the TES detectors to thermal bath fluctuations was simulated using the `xifusim` X-IFU readout chain simulator [8]. To do so, we modeled the wafer response as a change of the bath temperature of the pixels, assuming that the detector reaction does not influence the propagation of the heat wave. This constitutes a worst case as the TES response can only absorb part of the wave's energy. Fig. 4 (left) compares the response of an X-IFU pixel to a CR impact to that of a normal X-ray pulse. We see that the TES reacts much more slowly to the former than to the latter (∼5 times longer 90 % rise time). This is due to the fact that a bath temperature fluctuation has to go through the weak SiN thermal link to reach the TES when an X-ray photon directly thermalizes in the detector.

We further characterized the effect of thermal pulses on the energy measurement by simulating the energy error induced on a 7 keV X-ray pulse as a function of the time separation between the CR and photon hits (see Fig. 4, middle and right). The characteristic shape of

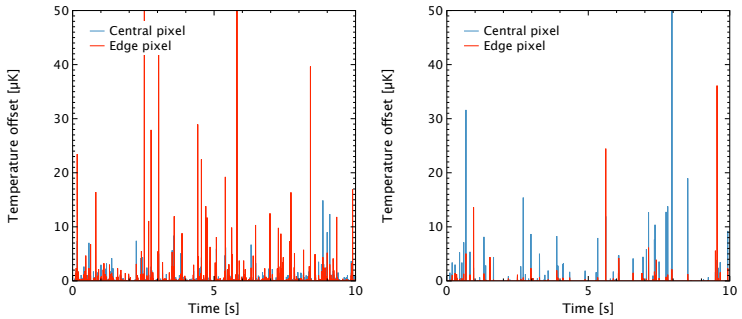

Fig. 5 Example of bath temperature timelines for the baseline wafer configuration. *Left:* For CR hits in the Si frame. *Right:* For CR hits in the muntin structure. (Color figure online)

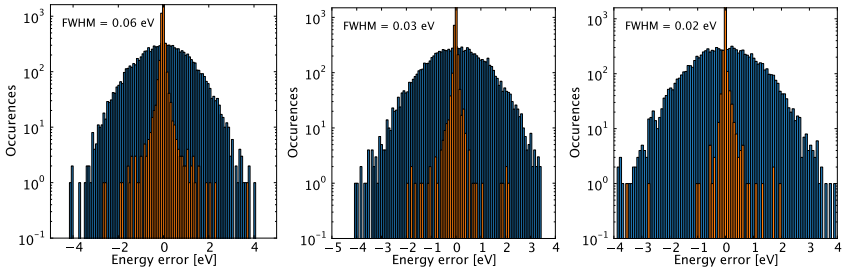

Fig. 6 Histogram of the energy errors induced by cosmic ray hits in 3 simulation scenarios (orange). For comparison, a realization of the 2.5 eV FWHM instrument gaussian broadening is shown in blue. The quoted FWHM values were measured from the 88th and 12th percentiles of the distribution. The rarest, largest energy errors (some eVs) are not plotted for visibility purposes (4, 1 and 5 events for the left, middle and right histograms respectively). *Left:* Frame hits for a side (worst case) pixel and the baseline heatsinking design. *Middle:* Same CR hits and victim pixel but with the optimized design. *Right:* Muntin hits for the central pixel (worst case). (Color figure online)

this time dependence is due to the shape of the optimal filter used and is similar to what is seen e.g. for crosstalk effects [9]. We see that significant energy errors can only occur within a few ms time coincidence. This will be quite common for the numerous frame hits, but with only 7 muntin hits per second (see Fig. 1, right), the likelihood of such an overlap is very limited.

3.2 Average energy resolution degradation

To estimate the overall effect on the X-IFU energy resolution of multiple CR impacts, it is necessary to simulate the TES response to not only single temperature profiles but to a complete bath temperature timeline. Such a timeline can be generated as follows: for each CR impact, its arrival time is drawn randomly from a Poisson distribution and its deposition energy selected from the relevant Geant4 CR event list. The location of the energy deposition is then selected uniformly over the wafer, assuming a flat spatial distribution. We then interpolate the induced temperature fluctuation using the pre-calculated temperature profiles obtained at different locations on the wafer (see Section 2.2). Finally, all resulting wafer re-

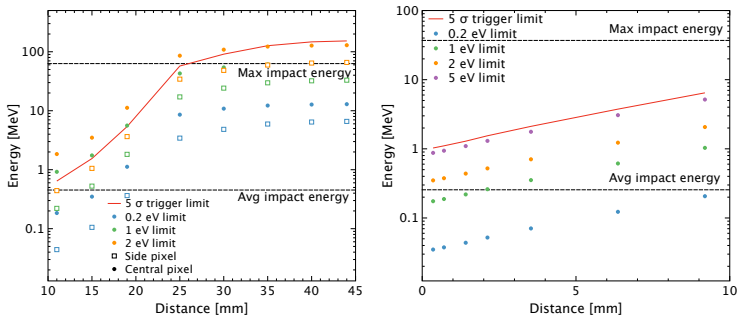

Fig. 7 Comparison between the 5 σ trigger level and the energy at which a CR deposition can induce different energy offsets. *Left:* Comparison made for hits in the frame and the baseline heatsinking design. The trigger pixel is assumed to be on the edge of the array. *Right:* Comparison made for hits in the muntin structure for a pixel and its trigger located at the center of the array. (Color figure online)

sponses are rescaled with energy and added together as the thermal model was found to be linear (see [6] and [7]). Fig. 5 shows examples of such timelines for CR hits both in the Si frame and in the muntin structure. We can see that fluctuations as high as few tens of µK are already quite common in 10 s long simulations. We further note that a pixel on the edge of the array will see larger fluctuations from the frame than one in the center of the array and inversely for hits in the muntins.

We thus simulated for all configurations a series of 10 000 such timelines, and modeled their impact on a concomitant 7 keV X-ray event. Figure 6 (left) shows the distribution of the measured energy reconstruction errors for frame hits in the baseline heatsinking configuration and for a pixel on the edge of the array (constitutes a worst case compared to the central one). We see that the distribution is largely non-Gaussian, but features a small inner broadening of 0.06 eV FWHM, well within the corresponding 0.2 eV allocation in the X-IFU energy resolution budget. Errors larger than this 0.2 eV limit only represent 1.2 % of the distribution. When comparing against a realization of the 2.5 eV instrument resolution Gaussian broadening, we see that these larger offsets will induce negligible non-gaussianities. Fig. 6 (middle) gives the same distribution for the optimized configuration, showing that it could offer a factor of two improvement in resolution degradation. Finally, we see from Fig. 6 (right) that hits in the muntin structure lead to an even narrower broadening due to the low associated CR count rate.

4 Triggering capability

As seen in the previous section, the most energetic CR energy depositions may lead to energy errors in the few eV range when coincident with a reconstructed X-ray event. Ideally, we would want such large errors to be flagged out from the scientific data. Due to the much slower rise of the pixel response to a bath temperature change than to an X-ray (see Fig. 4, left), the standard X-IFU trigger mechanism, however, cannot efficiently detect even the largest signals. We found through simulation that the optimal signal to noise ratio for thermal events is actually obtained for a pixel timeline filtered with a $\sim$ 1 ms averaging window (for comparison, the standard trigger operates with a 12.8 µs window).

To quantify this trigger's efficiency, we compared its 5 σ threshold level with the energy deposition required to induce various energy offsets on coincident X-rays. As seen in Fig. 7 (left), for the baseline heatsinking design, a trigger on an edge pixel could allow removing all energy offsets larger than $\sim$1 eV for central pixels and $\sim$ 2.5 eV for its neighboring pixels. Assuming a 2 ms exclusion window applied to the full array when an event is detected, this would be achieved with an almost negligible dead time penalty ($<$0.1 %). This solution is therefore attractive, but may not be strictly needed as shown in the previous section. A better solution may be to instead download a down-sampled timeline of a selection of pixels to more generally monitor any low-frequency environmental variations. This will be investigated in subsequent studies. This could allow partially correcting for the largest muntin hits, for which a simple trigger appears to be mostly ineffective (see Fig. 7, right).

5 Conclusion

In this paper, we investigated through simulations how the thermal fluctuations induced by cosmic ray hits on the X-IFU TES array Si wafer could affect the instrument energy resolution. We showed that with the baseline heatsinking design, this effect should remain well below its corresponding allocation in the instrument resolution budget and introduce negligible non-Gaussianities in the detector's response. An optimized heatsinking configuration can further reduce this effect by a factor of two. We also showed that a dedicated trigger mechanism operating on the edge pixels of the array could detect and veto some of the most energetic frame events. Of course, this purely model-based study now warrants a dedicated experimental verification, which shall be conducted in the current phase B of the X-IFU project. This may for instance include the measurement of the TESs response to individual energy depositions at known locations in the wafer using radioactive alpha sources and/or heaters and a comparison with the corresponding model. A first attempt at such a comparison was made with an *Hitomi/SXS* [10] wafer and showed encouraging results (see more details in [7]).

Acknowledgements This work has been partially funded by the Bundesministerium für Wirtschaft und Technologie under Deutsches Zentrum für Luft- und Raumfahrt grant 50 QR 1903.

References

1. K. Nandra, D. Barret, X. Barcons, A. Fabian, J.-W. den Herder, L. Piro, M. Watson, C. Adami, J. Aird, J. M. Afonso, and et al. The Hot and Energetic Universe: A White Paper presenting the science theme motivating the Athena+ mission. *ArXiv e-prints*, , June 2013.
2. Didier Barret, Thien Lam Trong, Jan-Willem den Herder, Luigi Piro, Massimo Cappi, Juhani Houvelin, Richard Kelley, J. Miguel Mas-Hesse, Kazuhisa Mitsuda, Stéphane Paltani, Gregor Rauw, Agata Rozanska, Joern Wilms, Simon Bandler, Marco Barbera, Xavier Barcons, Enrico Bozzo, Maria Teresa Ceballos, Ivan Charles, Elisa Costantini, Anne Decourchelle, Roland den Hartog, Lionel Duband, Jean-Marc Duval, Fabrizio Fiore, Flavio Gatti, Andrea Goldwurm, Brian Jackson, Peter Jonker, Caroline Kilbourne, Claudio Macculi, Mariano Mendez, Silvano Molendi, Piotr Orleanski, François Pajot, Etienne Pointecouteau, Frederick Porter, Gabriel W. Pratt, Damien Prêle, Laurent Ravera, Kosuke Sato, Joop Schaye, Keisuke Shinozaki, Tanguy Thibert, Luca Valenziano, Véronique Valette, Jacco Vink, Natalie Webb, Michael Wise, Noriko Yamasaki, Françoise Douchin, Jean-Michel Mesnager, Bernard Pontet, Alice Pradines, Graziella Branduardi-Raymont, Esra Bulbul, Mauro Dadina, Stefano Ettori, Alexis Finoguenov, Yasushi Fukazawa, Agnieszka Janiuk, Jelle Kaastra, Pasquale Mazzotta, Jon Miller, Giovanni Miniutti, Yael Naze, Fabrizio Nicastro, Salavtore Scioritino, Aurora Simonescu, Jose Miguel Torrejon, Benoit Frezouls, Hervé Geoffray, Philippe Peille, Corinne Aicardi, Jérôme André, Christophe Daniel, Antoine Clénet, Christophe Etcheverry, Emilie Gloaguen, Gilles Hervet, Antoine Jolly, Aurélien Ledot, Irwin Paillet, Roseline Schmisser, Bruno Vella, Jean-Charles Damery, Kevin Boyce, Mike Dipirro, Simone Lotti, Denis Schwander, Stephen Smith, Bert-Joost Van Leeuwen, Henk van Weers, Nicolas Clerc, Beatriz Cobo, Thomas Dauser, Christian Kirsch, Edoardo Cucchetti, Megan Eckart, Philippe Ferrando, and Lorenzo Natalucci. The ATHENA X-ray Integral Field Unit (X-IFU). In *Proc. SPIE*, volume 10699 of *Society of Photo-Optical Instrumentation Engineers (SPIE) Conference Series*, page 106991G, Jul 2018. doi: 10.1117/12.2312409.
3. S. Lotti and et al. Estimates for the background of the ATHENA X-IFU instrument: the Cosmic Rays contribution. In *Space Telescopes and Instrumentation 2018: Ultraviolet to Gamma Ray*, volume 10699 of *Proc. SPIE*, pages 10699–61, July 2018.
4. Matteo D'Andrea, Claudio Macculi, Andrea Argan, Simone Lotti, Gabriele Minervini, Luigi Piro, Michele Biasotti, Valentina Ceriale, Giovanni Gallucci, Flavio Gatti, Guido Torrioli, and Angela Volpe. The cryogenic anticoincidence detector for ATHENA X-IFU: preliminary test of AC-S9 towards the demonstration model. In *Proc. SPIE*, volume 10699 of *Society of Photo-Optical Instrumentation Engineers (SPIE) Conference Series*, page 106994T, Jul 2018. doi: 10.1117/12.2313280.
5. Planck Collaboration, P. A. R. Ade, N. Aghanim, C. Armitage-Caplan, M. Arnaud, M. Ashdown, F. Atrio-Barand ela, J. Aumont, C. Baccigalupi, A. J. Banday, R. B. Barreiro, E. Battaner, K. Benabed, A. Benoît, A. Benoit-Lévy, J. P. Bernard, M. Bersanelli, P. Bielewicz, J. Bobin, J. J. Bock, J. R. Bond, J. Borrill, F. R. Bouchet, M. Bridges, M. Bucher, C. Burigana, J. F. Cardoso, A. Catalano, A. Challinor, A. Chamballu, H. C. Chiang, L. Y. Chiang, P. R. Christensen, S. Church, D. L. Clements, S. Colombi, L. P. L. Colombo, F. Couchot, A. Coulais, B. P. Crill, A. Curto, F. Cuttaia, L. Danese, R. D. Davies, P. de Bernardis, A. de Rosa, G. de Zotti, J. Delabrouille, J. M. Delouis, F. X. Désert, J. M. Diego, H. Dole, S. Donzelli, O. Doré, M. Douspis, X. Dupac, G. Efstathiou, T. A. Enßlin, H. K. Eriksen, F. Finelli, O. Forni, M. Frailis, E. Franceschi,

S. Galeotta, K. Ganga, M. Giard, D. Girard, Y. Giraud-Héraud, J. González-Nuevo, K. M. Górski, S. Gratton, A. Gregorio, A. Gruppuso, F. K. Hansen, D. Hanson, D. Harrison, S. Henrot-Versillé, C. Hernández-Monteagudo, D. Herranz, S. R. Hildebrandt, E. Hivon, M. Hobson, W. A. Holmes, A. Hornstrup, W. Hovest, K. M. Huffenberger, A. H. Jaffe, T. R. Jaffe, W. C. Jones, M. Juvela, E. Keihänen, R. Keskitalo, T. S. Kisner, R. Kneissl, J. Knoche, L. Knox, M. Kunz, H. Kurki-Suonio, G. Lagache, J. M. Lamarre, A. Lasenby, R. J. Laureijs, C. R. Lawrence, R. Leonardi, C. Leroy, J. Lesgourgues, M. Liguori, P. B. Lilje, M. Linden-Vørnle, M. López-Caniego, P. M. Lubin, J. F. Macías-Pérez, N. Mandolesi, M. Maris, D. J. Marshall, P. G. Martin, E. Martínez-González, S. Masi, M. Massardi, S. Matarrese, F. Matthai, P. Mazzotta, P. McGehee, A. Melchiorri, L. Mendes, A. Mennella, M. Migliaccio, A. Miniussi, S. Mitra, M. A. Miville-Deschênes, A. Moneti, L. Montier, G. Morgante, D. Mortlock, S. Mottet, D. Munshi, J. A. Murphy, P. Naselsky, F. Nati, P. Natoli, C. B. Netterfield, H. U. Nørgaard-Nielsen, F. Noviello, D. Novikov, I. Novikov, S. Osborne, C. A. Oxborrow, F. Paci, L. Pagano, F. Pajot, D. Paoletti, F. Pasian, G. Patanchon, O. Perdereau, L. Perotto, F. Perrotta, F. Piacentini, M. Piat, E. Pierpaoli, D. Pietrobon, S. Plaszczynski, E. Pointecouteau, G. Polenta, N. Ponthieu, L. Popa, T. Poutanen, G. W. Pratt, G. Prézeau, S. Prunet, J. L. Puget, J. P. Rachen, B. Racine, M. Reinecke, M. Remazeilles, C. Renault, S. Ricciardi, T. Riller, I. Ristorcelli, G. Rocha, C. Rosset, G. Roudier, B. Rusholme, L. Sanselme, D. Santos, A. Sauvé, G. Savini, D. Scott, E. P. S. Shellard, L. D. Spencer, J. L. Starck, V. Stolyarov, R. Stompor, R. Sudiwala, F. Sureau, D. Sutton, A. S. Suur-Uski, J. F. Sygnet, J. A. Tauber, D. Tavagnacco, L. Terenzi, L. Toffolatti, M. Tomasi, M. Tristram, M. Tucci, G. Umana, L. Valenziano, J. Valiviita, B. Van Tent, P. Vielva, F. Villa, N. Vittorio, L. A. Wade, B. D. Wandelt, D. Yvon, A. Zacchei, and A. Zonca. Planck 2013 results. X. HFI energetic particle effects: characterization, removal, and simulation. *A&A*, 571:A10, Nov 2014. doi: 10.1051/0004-6361/201321577.

6. S. L. Stever, P. Peille, R. den Hartog, M. P. Bruijn, A. Roussaffi, S. Lotti, C. Macculi, and R. M. J. Janssen. Thermal simulations of temperature excursions on the athena x-ifu detector wafer from impacts by cosmic rays. *J. Low Temp. Phys.*, **This Special Issue**, 2019.
7. A. Miniussi, J. S. Adams, S. R. Bandler, S. Beaumont, M. P. Chang, J. A. Chervenak, F. M. Finkbeiner, J. Y. Ha, R. Hummatov, R. L. Kelley, C. A. Kilbourne, F. S. Porter, J. E. Sadleir, K. Sakai, S. J. Smith, N. A. Wakeham, and E. J. Wassel. Thermal impact of cosmic ray interaction with x-ray microcalorimeter array. *J. Low Temp. Phys.*, **This Special Issue**, 2019.
8. M. Lorenz, C. Kirsch, P. E. Merino-Alonso, P. Peille, S. J. Smith, and J. Wilms. Gpu supported simulation of transition-edge sensor arrays. *J. Low Temp. Phys.*, **This Special Issue**, 2019.
9. Philippe Peille, T. Dauser, C. Kirsch, R. den Hartog, E. Cucchetti, J. Wilms, D. Barret, J.-W. den Herder, and L. Piro. The performance of the athena x-ray integral field unit at very high count rates. *Journal of Low Temperature Physics*, May 2018. ISSN 1573-7357. doi: 10.1007/s10909-018-1964-6. URL `https://doi.org/10.1007/s10909-018-1964-6`.
10. K. Mitsuda, R. L. Kelley, H. Akamatsu, T. Bialas, K. R. Boyce, G. V. Brown, E. Canavan, M. Chiao, E. Costantini, J.-W. den Herder, C. de Vries, M. J. DiPirro, M. E. Eckart, Y. Ezoe, R. Fujimoto, D. Haas, A. Hoshino, K. Ishikawa, Y. Ishisaki, N. Iyomoto, C. A. Kilbourne, M. Kimball, S. Kitamoto, S. Konami, M. A. Leutenegger, D. McCammon, J. Miko, I. Mitsuishi, H. Murakami, M. Murakami, H. Noda, M. Ogawa, T. Ohashi, A. Okamoto, N. Ota, S. Paltani, F. S. Porter, K. Sato, Y. Sato, M. Sawada, H. Seta,

K. Shinozaki, P. J. Shirron, G. A. Sneiderman, H. Sugita, A. Szymkowiak, Y. Takei, T. Tamagawa, M. S. Tashiro, Y. Terada, M. Tsujimoto, S. Yamada, and N. Y. Yamasaki. Soft x-ray spectrometer (SXS): the high-resolution cryogenic spectrometer onboard ASTRO-H. In *Space Telescopes and Instrumentation 2014: Ultraviolet to Gamma Ray*, volume 9144 of *Proc. SPIE*, page 91442A, July 2014. doi: 10.1117/12.2057199.